Journal of Power Sources 196 (2011) 218–227

Contents lists available at ScienceDirect

Journal of Power Sources

journal homepage: www.elsevier.com/locate/jpowsour

Performance equations for a polymer electrolyte membrane fuel cell with unsaturated cathode feed

Hsiao-Kuo Hsuen, Ken-Ming Yin*

Department of Chemical Engineering, Yuan Ze University, 135 Yuan-Tung Road, Taoyuan, Chung-Li 32003, Taiwan, ROC

ARTICLE INFO

Article history:
Received 5 June 2010
Accepted 15 June 2010
Available online 23 June 2010

Keywords:
Polymer electrolyte membrane fuel cell
Performance equations
Modeling
Water saturation
Unsaturated cathode feed

ABSTRACT

A mathematical formulation for the cathode of a membrane electrode assembly of a polymer electrolyte membrane fuel cell is proposed, in which the effect of unsaturated vapor feed in the cathode is considered. This mechanistic model formulates the water saturation front within the gas diffusion layer with an explicit analytical expression as a function of operating conditions. The multi-phase flows of gaseous species and liquid water are correlated with the established capillary pressure equilibrium in the medium. In addition, less than fully hydrated water contents in the polymer electrolyte and catalyst layers are considered, and are integrated with the relevant liquid and vapor transfers in the gas diffusion layer. The developed performance equations take into account the influences of all pertinent material properties on cell performance using first principles. The mathematical approach is logical and concise in terms of revealing the underlying physical significance in comparison with many other empirical data fitting models.

1. Introduction

The proton exchange membrane fuel cell (PEMFC) is one of several possible candidates for the replacement of the internal combustion engine in automobiles to eliminate pollutant emissions. The capabilities of PEMFCs have been demonstrated as stationary residential and portable power sources [1]. The performance of a PEMFC depends on its well-designed membrane electrode assembly (MEA) to ensure optimized mass transport and electrochemical kinetics under voltage or current operating modes. Since most voltage consumption occurs in the cathode oxygen reduction reaction, as compared to the relatively facile hydrogen oxidation reaction, the cathode compartment of the MEA has been the focus of many theoretical and experimental studies [2,3]. Fig. 1 is a schematic of the cathode part of the MEA, which consists of a polymer electrolyte membrane, a cathode catalyst layer, and a cathode gas diffusion layer. The solid polymer electrolyte membrane plays the role of electrode separator between the anode and the cathode, as well as the proton transport vehicle. Fully dispersed platinum nano-particles supported by high surface carbon powders were fabricated in the catalyst layer to replace the previously used platinum black so that a greater active area per unit volume is available for the electrochemical reaction [4]. The gas diffusion layer (GDL), made of weaved carbon fibers, is usually hydrophobically treated to enhance its water repulsion capability. The GDL facilitates uniform oxygen mass transfer from the gas channel, and repulses water that is generated in the cathode catalyst layer and that is dragged from the polymer membrane by electro-osmosis [5]. The advancement of cell performance is hinged on a proper MEA fabrication technique with appropriate physical/chemical properties.

Many mathematical models have been proposed as diagnostic tools to evaluate MEA performance in practical operations. Two conceptually different approaches have appeared in the literature of PEMFC 1-D simulations, that is, the macro-homogeneous and the heterogeneous models. In the former, a mixture of carbon supported platinum catalysts (Pt/C), polymer electrolyte, and liquid water-filled pores is assumed to be in a single homogeneous phase within the catalyst layer [4–10]. In the latter, various types of agglomerates of mixed Pt/C and ionomers with different geometric dimensions are connected as a three-dimensional network in the catalyst layer [11–16]. Among the agglomerates, which may be covered with water, inter-particle gaseous oxygen diffusion occurs. In addition, gaseous oxygen needs to be dissolved on the external surface and diffuses to the interior of the agglomerates for the electrochemical reaction on the active Pt/C site. Both approaches have correlated well with experimental observations, except that the double Tafel slope phenomena observed in the cathodic polarization is better simulated using the agglomerate model [13]. Computational fluid dynamics techniques have been developed for 2-D and 3-D simulations with considerations of heat transfer [17–21], anisotropic material properties [22–24], and convective flow in the channel [25–27] with various degrees of

* Corresponding author. Tel.: +886 3 4638800x2556; fax: +886 3 4559373.
E-mail address: cekenyin@saturn.yzu.edu.tw (K.-M. Yin).

0378-7753/$ – see front matter © 2010 Elsevier B.V. All rights reserved.
doi:10.1016/j.jpowsour.2010.06.058

Nomenclature

a	effective platinum surface area per unit volume (cm^{-1})
a_0	specific platinum surface area (cm^{-1})
A	parameter in capillary pressure head expression, Eq. (27), dimensionless
c_{O_2}	oxygen concentration ($mol\,cm^{-3}$)
$c_{O_2,ref}$	reference oxygen concentration, defined as P/H_{O_2} ($mol\,cm^{-3}$)
C	parameter in capillary pressure head expression, Eq. (27), dimensionless
d_c	catalyst layer thickness (cm)
d_d	gas diffusion layer thickness (cm)
d_m	membrane thickness (cm)
d_w	width of the two-phase region within gas diffusion layer (cm)
D	parameter in capillary pressure head expression, Eq. (27) (cm)
D_{i-j}	binary diffusion coefficient for i and j species ($cm^2\,s^{-1}$)
D_{i-j}^{eff}	effective binary diffusion coefficient for i and j species ($cm^2\,s^{-1}$)
$D_{O_2}^{eff}$	effective diffusivity of dissolved oxygen in the catalyst layer ($cm^2\,s^{-1}$)
D_λ	water diffusivity in membrane ($cm^2\,s^{-1}$)
e	swelling expansion coefficient of membrane, dimensionless
f_c	parameter defined by Eq. (6c) (V^{-1})
F	Faraday's constant (96,487 C per equivalent)
g	gravitational acceleration ($980\,cm\,s^{-2}$)
H_{O_2}	Henry's constant for oxygen solubility ($atm\,cm^3\,mol^{-1}$)
$i_{o,ref}$	exchange current density at the reference condition ($A\,cm^{-2}$)
I	cathode current density ($A\,cm^{-2}$)
I_o	characteristic current density, defined by Eq. (6f) ($A\,cm^{-2}$)
$k_{p,m}$	membrane permeability (cm^2)
K	liquid water permeability in diffuser at partial saturated condition (cm^2)
$K_{l,abs}$	liquid water permeability in diffusion layer at fully saturation (cm^2)
m_m	membrane molecular weight ($g\,mol^{-1}$)
m_w	water molecular weight ($g\,mol^{-1}$)
n_d	electro-osmotic drag coefficient, defined by Eq. (21), dimensionless
N_i	mole flux of species i ($mol\,cm^{-2}\,s^{-1}$)
P	total pressure (atm)
ΔP_m	pressure difference between two sides of membrane in Eq. (18) ($g\,cm^{-1}\,s^{-2}$)
q_w	liquid water flux ($cm\,s^{-1}$)
R	universal gas constant ($8.314\,J\,mol^{-1}\,K^{-1}$)
s	liquid water saturation in diffusion layer, dimensionless
s^c	water saturation at the catalyst-layer/diffusion-layer interface, dimensionless
T	cathode temperature (K)
v_w	molar volume of water ($cm^3\,mol^{-1}$)
v_m	molar volume of dry membrane ($cm^3\,mol^{-1}$)
V	catalyst layer potential (V)
V_c	cathode potential (V)
V_o	open circuit potential (V)
x_i	mole fraction of species i, dimensionless
x_i^b	mole fraction of species i in channel, dimensionless
x_i^c	mole fraction of species i at the catalyst-layer/diffusion-layer interface, dimensionless
x_i^f	mole fraction of species i at the interface of single phase and two-phase regions, dimensionless
z	coordinate perpendicular to the face of the gas diffusion layer (cm)

Greek letters

α_c	cathodic transfer coefficient, dimensionless
β_1	parameter defined by Eq. (6b) ($S\,cm^{-2}$)
β_2	parameter defined by Eq. (13) ($S\,cm^{-2}$)
β_m	parameter defined by Eq. (53) ($S\,cm^{-2}$)
ε	gas void fraction in diffusion layer, dimensionless
ε_m	volume fraction of the ionomer phase in the catalyst layer, dimensionless
ε_0	porosity of gas diffusion layer at zero water saturation, dimensionless
$\varepsilon_{w,m}$	volume fraction of water in membrane, expressed by Eq. (22), dimensionless
ϕ	ionomer potential (V)
φ	parameter defined by Eq. (6a), dimensionless
ψ	capillary head (cm)
Λ	parameter defined by Eq. (48), dimensionless
η	parameter defined by Eq. (46), dimensionless
λ	water content in membrane (mole of water per mole of sulfonic groups), dimensionless
λ_s	saturated water content in membrane, dimensionless
μ_w	viscosity of liquid water ($g\,cm^{-1}\,s^{-1}$)
$\rho_{m,dry}$	density of dry membrane ($g\,cm^{-3}$)
ρ_w	density of liquid water ($g\,cm^{-3}$)
σ_d^{eff}	effective electric conductivity of the diffusion layer ($S\,cm^{-1}$)
σ_m	protonic conductivity of membrane ($S\,cm^{-1}$)
σ_m^{eff}	effective proton conductivity in the ionomer phase of catalyst layer ($S\,cm^{-1}$)
τ_w	water molar flux driven by hydraulic permeation, defined by Eq. (30) ($mol\,cm^{-2}\,s^{-1}$)

complexity. However, to facilitate a quick evaluation of single cell performance in a typical laboratory, it would be better to have a simple, versatile mechanistic model for the evaluation of MEA fabrication techniques. Srinivasan and co-workers [28–30] proposed a semi-empirical equation to describe the polarization behavior of PEMFCs that considers the effects of electrode activation overpotential and membrane ohmic resistance. This was the prototype of many later empirical PEMFC models [31–33]. Due to the inability of Srinivasan's equation to predict the limiting current behavior, an additional correction factor was incorporated by Squadrito et al. [31]. Other modifications to account for the mass transfer effect of the GDL at high current densities were made by Chu et al. [32] and Xia and Chan [33]. However, the proposed equations in those articles lack sound physical grounds for a detailed description of the associated electrochemical process, and the fitted parameters are only applicable to a very limited operating region. Hsuen [34–36] proposed a series of mechanistic models of the PEMFC that quantify all significant potential losses that stem from cell electrochemical resistances and transport hindrances. Specifically, the voltage drops are contributed to by gaseous mass transport in the gas diffusion layer, dissolved oxygen diffusion in the catalyst layer, electron transport of carbon fiber in the gas diffusion layer, electron trans-

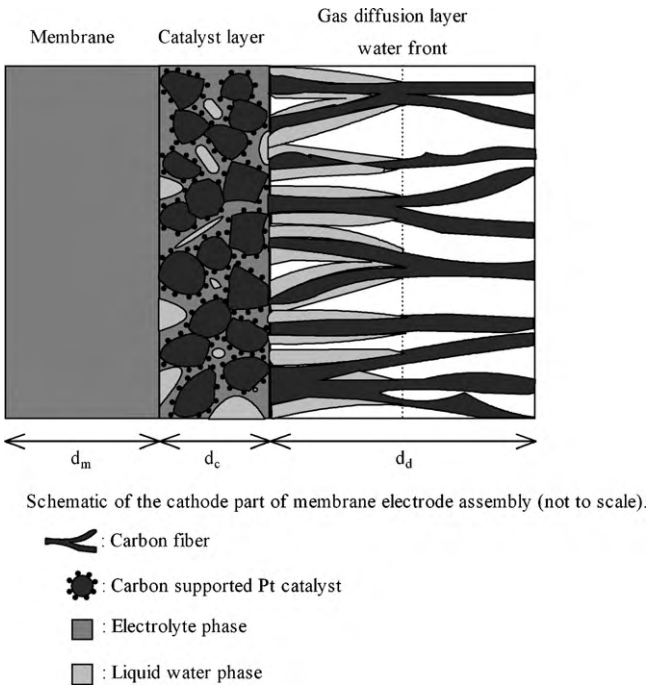

Fig. 1. Schematic diagram of the cathode part of membrane electrode assembly.

port of the Pt/C phase in the catalyst layer, the electrochemical reaction of oxygen reduction on the Pt/C surface, and proton migration within the polymer electrolyte phase. In addition, the influence of liquid water blockage on oxygen diffusion and cathode overpotential was quantified under a fully humidified air feed [36]. The concise, analytical while mechanistic formulated approach is extremely computationally efficient. It can be easily modified, if desired, with a parameter estimation scheme to retrieve useful kinetic properties of the MEA for possible fabrication improvement. The present work is a further extension of previous developments to include the case of unsaturated air feed in the cathode. It is shown that the position of the water saturation front in the gas diffusion layer can be explicitly identified based on the analytically derived equations. In addition, a less than fully hydrated polymer electrolyte membrane, and the associated water diffusion and electro-osmotic drag, are incorporated in the model. The proposed mechanistic model is more versatile and realistic in terms of the evaluation of kinetic/transport parameters for a better membrane electrode assembly design when compared to other empirical data fitting models of limited applicability.

2. Mathematical model

The mathematical model for the PEMFC cathodes considered in the present work is a steady-state, one-dimensional, and isothermal model. The schematic diagram of the system is illustrated in Fig. 1. The system is composed of a membrane, a cathode catalyst layer, and the adjacent gas diffusion layer. In the catalyst layer, the macro-homogeneous assumption is applied. This assumption implies constant physical and chemical properties within the layer, and that catalyst particles, in the form of platinum clusters supported on carbon black, are well mixed with proton-conductive ionomers. In addition, the water content of the ionomer phase within the catalyst layer is considered to be invariant with position. Since the electrochemical reaction takes place at the interface between the platinum clusters and ionomers, oxygen molecules have to be dissolved into the ionomer phase before reacting with protons. Other assumptions used in formulating the model equations are delineated as follows:

(i) The ideal gas law is applied for the gaseous species within the gas diffusion layer.
(ii) The total gas pressure within the gas diffusion layer is constant.
(iii) The Stefan–Maxwell equations are used to describe multi-component gas transport in the gas diffusion layer, and the effective binary gas diffusivities are evaluated using the Bruggeman expression [4].
(iv) The interfacial surface area for the liquid and vapor phases of water in the diffusion layer is large enough such that the water vapor is saturated in the presence of liquid water.
(v) The membrane is impermeable to gaseous species and dissolved oxygen.
(vi) The nitrogen mole flux is zero due to its inertness and assumption (v).
(vii) The rate form of oxygen reduction follows a first-order expression with respect to oxygen concentration. In addition, the reaction rate is described by the Tafel expression [37].
(viii) The phase equilibrium of oxygen at the catalyst-layer/diffusion-layer interface is achieved and follows Henry's law [4].
(ix) Convective mass transfer of dissolved oxygen in the catalyst layer is negligible due to small values of its mole fraction in the mobile phase, and Fick's law is applied to describe the transport of dissolved oxygen within the catalyst layer.
(x) The potential loss due to electron conduction in the catalyst layer is considered to be negligible.
(xi) The effects of various flow field designs are not included in the present model. That is, only the mass transport normal to the membrane electrode assembly is considered.

2.1. Model equations with no liquid water in the gas diffusion layer (Case I)

Under the condition that liquid water is not present in the gas diffusion layer, the Stefan–Maxwell equations take the forms

$$\frac{P}{RT}\frac{dx_w}{dz} = \left(\frac{N_{O_2}}{D^{eff}_{O_2-w}} + \frac{N_w}{D^{eff}_{N_2-w}}\right)x_w + N_w\left(\frac{1}{D^{eff}_{N_2-w}} - \frac{1}{D^{eff}_{O_2-w}}\right)x_{O_2} - \frac{N_w}{D^{eff}_{N_2-w}} \quad (1)$$

$$\frac{P}{RT}\frac{dx_{O_2}}{dz} = \left(\frac{N_{O_2}}{D^{eff}_{O_2-N_2}} + \frac{N_w}{D^{eff}_{O_2-w}}\right)x_{O_2} + N_{O_2}\left(\frac{1}{D^{eff}_{N_2-O_2}} - \frac{1}{D^{eff}_{O_2-w}}\right)x_w - \frac{N_{O_2}}{D^{eff}_{N_2-O_2}} \quad (2)$$

where N_i denotes the mole flux of species i, x_i its mole fraction, R the universal gas constant, P the total pressure, T the cathode temperature, and D^{eff}_{i-j} an effective gas-pair diffusivity for i and j species in the porous medium that is evaluated by

$$D^{eff}_{i-j} = D_{i-j}\varepsilon_0^{1.5} \quad (3)$$

in which ε_0 denotes the porosity of the diffusion layer.

In the catalyst layer, the equations of mass conservation and Ohm's law can be expressed in partially dimensionless form as [36]

$$\frac{d^2x_{O_2}}{dz^2} - \frac{\varphi}{d_c^2}\left\{\exp\left[f_c(V_0 - V + \phi)\right]\right\}x_{O_2} = 0 \quad (4)$$

$$\frac{d^2x_{O_2}}{dz^2} - \frac{\beta_1}{I_o}\frac{d^2\phi}{dz^2} = 0 \quad (5)$$

The model parameters appearing in the above expressions are defined by

$$\varphi = \frac{ai_{o,ref}H_{O_2}d_c^2}{4FPD_{O_2}^{eff}}; \quad \beta_1 = \frac{\sigma_m^{eff}}{d_c}; \quad f_c = \frac{\alpha_c F}{RT}$$

$$x_{O_2} = \frac{c_{O_2}}{c_{O_2,ref}} = \frac{c_{O_2}}{P/H_{O_2}}; \quad I_o = \frac{4FPD_{O_2}^{eff}}{H_{O_2}d_c} \tag{6a–f}$$

where α_c is the electrode transfer coefficient, a is the effective platinum surface area per unit volume, $i_{o,ref}$ is the exchange current density at the reference condition, c_{O_2} is the dissolved oxygen concentration in the ionomer phase, d_c is the catalyst-layer thickness, σ_m^{eff} is the effective protonic conductivity for the ionomer phase, $D_{O_2}^{eff}$ is the effective diffusivity of dissolved oxygen in the catalyst layer, F is the Faraday constant, P is the cathode pressure, V_o is the open-circuit potential, V is the catalyst potential, ϕ is the ionomer potential, and H_{O_2} is the Henry's constant for gaseous oxygen and its dissolved form in the ionomer phase at the cathode temperature. In the above expressions, x_{O_2} represents the mole fraction of gaseous oxygen in the gas diffusion layer, but stands for the dimensionless concentration of dissolved oxygen in the ionomer phase of the catalyst layer. The same notation is used because, by such definitions, in both regions the x_{O_2} profiles are continuous across their boundary.

At the face of the diffusion layer ($z = d_m + d_c + d_d$), it is assumed that mass transfer limitations are negligible and, thus, one has

$$x_{O_2} = x_{O_2}^b \tag{7}$$

$$x_w = x_w^b \quad \text{or} \quad x_{N_2} = x_{N_2}^b \tag{8a,b}$$

At the diffusion-layer/catalyst-layer interface ($z = d_m + d_c$), this requires that

$$x_{O_2}(\text{catalyst layer}) = x_{O_2}(\text{gas diffusion layer}) \tag{9}$$

$$\frac{I_o}{4F}\frac{dx_{O_2}}{dz}(\text{catalyst layer}) = \frac{I}{d_c} \tag{10}$$

$$\frac{d\phi}{dz} = 0 \tag{11}$$

The cathode potential (denoted as V_c) is equivalent to the catalyst potential minus the ohmic loss of the diffusion layer. Thus, one has

$$V_c = V(\text{catalyst}) - \frac{I}{\beta_2} \tag{12}$$

and

$$\beta_2 = \frac{\sigma_d^{eff}}{d_d} \tag{13}$$

where σ_d^{eff} is the effective electric conductivity of the diffusion layer and d_d its thickness. It is postulated that phase equilibrium is instantaneously established between the water vapor and the water content of the ionomer phase of the catalyst layer at the diffusion-layer/catalyst-layer interface, which follows [7]

$$\lambda = 0.043 + 17.8\left(\frac{x_w}{x_w^s}\right) - 39.8\left(\frac{x_w}{x_w^s}\right)^2 + 36.0\left(\frac{x_w}{x_w^s}\right)^3 \tag{14}$$

In addition, the value of the effective protonic conductivity for the ionomer phase, denoted as σ_m^{eff}, is evaluated by [7]

$$\sigma_m^{eff} = \varepsilon_m^{1.5}(0.00514\lambda - 0.00326)\exp\left[1268\left(\frac{1}{303} - \frac{1}{T}\right)\right] \tag{15}$$

where ε_m represents the volume fraction of the ionomer phase in the catalyst layer. For the electrochemical reaction occurring within the catalyst layer, the surfaces of the platinum clusters are effective for the reaction only if they are in intimate contact with dissolved oxygen and protons. In other words, the platinum surface, which is not covered by hydrated ionomers, is considered to be inactive for the reaction. Therefore, as the water content of the ionomer phase within the catalyst layer is decreased, the amount of active surface area of the platinum clusters is expected to decrease as well. In the present work, a linear equation is employed as a first approximation to account for such an observation, that is

$$a = a_0\left(\frac{\lambda}{\lambda_s}\right), \tag{16}$$

in which λ_s is the value of λ at $x_w = x_w^s$ and a_0 is the specific platinum surface area.

It is postulated that the membrane is impermeable to oxygen; thus, one has

$$\frac{dx_{O_2}}{dz} = 0 \tag{17}$$

at the membrane/catalyst-layer interface ($z = d_m$).

As stated above, the membrane is assumed to be impermeable to gaseous species. However, as a pressure difference is applied to the both sides of the membrane, flow of liquid water is induced by the pressure gradients within the membrane, which can be quantitatively described by Darcy's law. In addition, electro-osmotic drag caused by proton flow and back diffusion resulting from the gradients of water concentration also significantly contribute to the overall water flux within the membrane. Accordingly, the water transport equation within the membrane can be formulated by [36].

$$N_w + 2N_{O_2} = n_d\frac{I}{F} - \frac{\rho_{m,dry}}{m_m}D_\lambda\frac{d\lambda}{dz} - \frac{\varepsilon_{w,m}\rho_w k_{p,m}}{m_w\mu_w(1+e\lambda)}\frac{\Delta P_m}{d_m} \tag{18}$$

where e (=0.0126) is the swelling expansion coefficient of the membrane, according to Springer et al. [7], m_m is the molecular weight of the membrane, n_d denotes the electro-osmotic drag coefficient, λ is the water content in membrane, D_λ is the water diffusivity, $k_{p,m}$ is the membrane permeability, d_m is the membrane thickness, I is the current density, μ_w is the water viscosity, ρ_w is the water density, m_w is the molecular weight of water, $\varepsilon_{w,m}$ is the volume fraction of water in membrane, and ΔP_m is the pressure difference between the two sides of the membrane. The value of $\rho_{m,dry}/m_m$ is $1/v_m = 1/550\ \text{mol cm}^{-3}$, where v_m denotes the molar volume of the dry membrane. The water diffusivity is evaluated using [7]

$$D_\lambda = D_\lambda(303\ \text{K})\ \exp\left[2416\left(\frac{1}{303} - \frac{1}{T}\right)\right] \tag{19}$$

in which

$$D_\lambda(303\ \text{K}) = (-2.86 + 1.89\lambda)\times 10^{-6}, \quad 2 \le \lambda < 3$$

$$D_\lambda(303\ \text{K}) = (6.38 - 1.19\lambda)\times 10^{-6}, \quad 3 \le \lambda < 4$$

$$D_\lambda(303\ \text{K}) = \left(2.563 - 0.33\lambda + 0.0264\lambda^2 - 0.000671\lambda^3\right)\times 10^{-6}, \quad 4 \le \lambda \tag{20a–c}$$

The electro-osmotic drag coefficient is calculated as [7]

$$n_d = 2.5\frac{\lambda}{22} \tag{21}$$

and the volume fraction of water in the membrane is estimated from Hsing and Peter [38]

$$\varepsilon_{w,m} = \frac{(\lambda - 1)v_w}{v_m + \lambda v_w} \tag{22}$$

where v_w is the molar volume of water.

At the exterior boundary of the membrane ($z = 0$), the boundary conditions are formulated as

$$\lambda = \lambda_s \quad \text{and} \quad \phi = 0 \tag{23a,b}$$

2.2. Model equations with liquid water in the gas diffusion layer (Case II)

As liquid water appears in the gas diffusion layer, the diffusion layer can be considered to consist of two regions, namely a one-phase region and a two-phase region. In the one-phase region, the Stefan–Maxwell equations derived above are also applicable. Since the gradients of the mole fraction of water vapor in the two-phase region become vanishingly small, the Stefan–Maxwell equations can be further condensed to one equation, which is

$$\frac{P}{RT}\frac{dx_{O_2}}{dz} = -(1 - x_w^s - x_{O_2})N_{O_2} \times \left[\frac{1}{D_{N_2-O_2}^{eff}} + \frac{x_w^s}{x_{O_2}D_{w-N_2}^{eff} + (1 - x_w^s - x_{O_2})D_{O_2-w}^{eff}}\right] \tag{24}$$

The effective gas-pair diffusivity needs to be modified by the water saturation, s, using the Bruggeman relation

$$D_{i-j}^{eff} = D_{i-j}\varepsilon_0^{1.5}(1 - s)^{1.5} \tag{25}$$

In addition, the transport equations for liquid water within the diffusion layer are also needed for the overall water balance. Darcy's law was employed to describe the liquid water transport in the diffusion layer. Because it is postulated that the variations of gas pressure within the diffusion layer are negligible, the gradients of capillary pressure of the liquid phase become the only driving forces for the flow of liquid water. Capillary head, indicated as ψ, is the driving force for water flux q_w.

$$q_w = -\frac{K(s)\rho_w g}{\mu_w}\left(-\frac{d\psi}{ds}\right)\frac{ds}{dz} \tag{26}$$

where $K(s)$ is the diffusion layer permeability and g is the gravitational acceleration.

$d\psi/ds$ and $K(s)$ are expressed as [39]

$$\frac{d\psi}{ds} = -AD\left[e^{-A(s-c)} + e^{A(s-c)}\right] \tag{27}$$

$$K(s) = K_{l,abs}(s + 0.01) \tag{28}$$

where $K_{l,abs}$ is the absolute diffusion layer permeability. The overall water balance within the diffusion layer requires [36]

$$[(2 + 4n_d)N_{O_2} + N_w + \tau_w]\left(\frac{m_w}{\rho_w}\right) + \frac{-K(s)\rho_w g}{\mu_w}\left(\frac{-d\psi}{ds}\right)\left(\frac{ds}{dz}\right) = 0 \tag{29}$$

and τ_w denotes

$$\tau_w = \frac{\rho_w k_{p,m}(\lambda_s - 1)\nu_w \Delta P_m}{m_w \mu_w (\nu_m + \lambda_s \nu_w)(1 + e\lambda_s)d_m} \tag{30}$$

At the boundary between these two regions, this requires that $x_w = x_w^s$ as well as the continuation of x_{O_2} and x_{N_2}. The governing equations for the catalyst layer remain the same except that the water content of the ionomer phase reaches its saturated value. In addition, the water transport equation for the membrane is no longer needed since the profile of the water content within it becomes uniform.

3. Cathode potential

3.1. Solutions for the case without liquid water in the gas diffusion layer

The value of current density, denoted as I, can be related to N_{O_2} as

$$N_{O_2} = -\frac{I}{4F} \tag{31}$$

The magnitudes of D_{N_2-w} and D_{O_2-w} only differ by about 7% due to the similar molecular weights of oxygen and nitrogen. With the aid of the approximation $D_{N_2-w}^{eff} \cong D_{O_2-w}^{eff}$ and Eq. (31), Eq. (1) can be further simplified as

$$\frac{P}{RT}\frac{dx_w}{dz} = \left(\frac{4FN_w - I}{4FD_{O_2-w}^{eff}}\right)x_w - \frac{N_w}{D_{O_2-w}^{eff}} \tag{32}$$

Hsuen [36] showed that this approximation greatly facilitates the simplification but without introducing appreciable errors.

Eq. (32) is solved analytically to give

$$x_w = \frac{4FN_w}{4FN_w - I} - \left(x_{O_2}^b + x_{N_2}^b + \frac{I}{4FN_w - I}\right) \times \exp\left[(z - d_m - d_c - d_d)\frac{RT}{PD_{O_2-w}^{eff}}\left(N_w - \frac{I}{4F}\right)\right] \tag{33}$$

The solution of Eq. (2) can be obtained by substituting Eq. (33) into it, which yields

$$x_{O_2} = -x_{N_2}^b \exp\left[(z - d_m - d_c - d_d)\frac{RT}{P}\left(\frac{-I}{4FD_{O_2-N_2}^{eff}} + \frac{N_w}{D_{O_2-w}^{eff}}\right)\right] - \frac{I}{4FN_w - I} + \left(x_{O_2}^b + x_{N_2}^b + \frac{I}{4FN_w - I}\right) \times \exp\left[(z - d_m - d_c - d_d)\frac{RT}{PD_{O_2-w}^{eff}}\left(N_w - \frac{I}{4F}\right)\right] \tag{34}$$

Then, the value of x_w, denoted as x_w^c, at the catalyst-layer/diffusion-layer interface ($z = d_m + d_c$) is readily calculated as

$${x_w}^c = \frac{4FN_w}{4FN_w - I} - \left(x_{O_2}^b + x_{N_2}^b + \frac{I}{4FN_w - I}\right)\exp\left[\frac{-d_d RT}{PD_{O_2-w}^{eff}}\left(N_w - \frac{I}{4F}\right)\right] \tag{35}$$

For fixed values of I and N_w, Eqs. (18)–(23a) form an initial value problem with one state variable λ. In the present work, the integration of Eq. (18) from the membrane exterior boundary ($z = 0$) to the catalyst-layer/membrane interface ($z = d_m$) is carried out using an explicit Euler method. After the integration, I remains unchanged while N_w is adjusted, and the above integration procedures are repeated until the value of λ at $z = d_m$ matches the value estimated using Eqs. (14) and (35) within the desired tolerance. Since only one unknown, N_w, is to be solved, a bisection method is employed for iterations. As the value of N_w is determined for a given I, the values of x_{O_2} and x_{N_2} at the diffusion-layer/catalyst-layer interface ($z = d_m + d_c$), indicated as $x_{O_2}^c$ and $x_{N_2}^c$, are then calculated as

$$x_{O_2}^c = -x_{N_2}^b \exp\left[\frac{-d_d RT}{P}\left(\frac{-I}{4FD_{O_2-N_2}^{eff}} + \frac{N_w}{D_{O_2-w}^{eff}}\right)\right] - \frac{I}{4FN_w - I} + \left(x_{O_2}^b + x_{N_2}^b + \frac{I}{4FN_w - I}\right) \times \exp\left[\frac{-d_d RT}{PD_{O_2-w}^{eff}}\left(N_w - \frac{I}{4F}\right)\right] \tag{36}$$

$$x^c_{N_2} = x^b_{N_2} \exp\left[\frac{-d_d RT}{P}\left(\frac{-I}{4FD^{eff}_{O_2-N_2}} + \frac{N_w}{D^{eff}_{O_2-w}}\right)\right] \quad (37)$$

3.2. Solutions for the case with liquid water in the gas diffusion layer

Under the condition that liquid water appears in the gas diffusion layer, the width of the two-phase region, denoted as d_w, can be directly calculated using Eqs. (18), (31) and (33) by assigning the mole fraction of water vapor at the boundary of the one-phase and the two-phase regions to its saturated value, which yields

$$d_w = d_d - \frac{4FPD^{eff}_{O_2-w}}{RT\,[(4n_d+1)I-4F\tau_w]} \ln\left\{\frac{[(4n_d+1)I-4F\tau_w](1-x^b_w)+I}{[(4n_d+1)I-4F\tau_w](1-x^s_w)+I}\right\} \quad (38)$$

The mole fraction of x_{O_2} and x_{N_2} at the boundary of these two regions, denoted as $x^f_{O_2}$ and $x^f_{N_2}$, are readily determined using Eqs. (34) and (33), and the constraint of $1 = x^f_{N_2} + x^f_{O_2} + x^f_w$, which give

$$x^f_{O_2} = -x^b_{N_2} \exp\left\{-(d_d - d_w)\frac{RT}{4FP}\left[\frac{-I}{D^{eff}_{O_2-N_2}} + \frac{(4n_d+2)I-4F\tau_w}{D^{eff}_{O_2-w}}\right]\right\} - \frac{I}{(4n_d+1)I-4F\tau_w} + \left[x^b_{O_2} + x^b_{N_2} + \frac{I}{(4n_d+1)I-4F\tau_w}\right] \times \exp\left\{-(d_d-d_w)\frac{RT\,[(4n_d+1)I-4F\tau_w]}{4FPD^{eff}_{O_2-w}}\right\} \quad (39)$$

$$x^f_{N_2} = x^b_{N_2} \exp\left\{\frac{-(d_d-d_w)RT}{4FP}\left[\frac{-I}{D^{eff}_{O_2-N_2}} + \frac{(4n_d+2)I-4F\tau_w}{D^{eff}_{O_2-w}}\right]\right\} \quad (40)$$

In the two-phase region, the Stefan–Maxwell equations can be rearranged from Eq. (1) to give

$$N_w = N_{O_2}\left[\frac{D^{eff}_{N_2-w}x^s_w}{D^{eff}_{N_2-w}x_{O_2} + D^{eff}_{O_2-w}\left(1-x^s_w-x_{O_2}\right)}\right] = N_{O_2}\left[\frac{D_{N_2-w}x^s_w}{D_{N_2-w}x_{O_2} + D_{O_2-w}\left(1-x^s_w-x_{O_2}\right)}\right] \quad (41)$$

With the approximation $D^{eff}_{N_2-w} \cong D^{eff}_{O_2-w}$, Eq. (41) is further simplified to

$$N_w = N_{O_2}\left(\frac{x^s_w}{1-x^s_w}\right) \quad (42)$$

Inserting Eq. (42) into Eq. (29), the overall water conservation within the diffusion layer results

$$\left[(2+4n_d) + \frac{D_{N_2-w}x^b_w}{D_{N_2-w}x_{O_2} + D_{O_2-w}(1-x^b_w-x_{O_2})}\right]N_{O_2} + \tau_w - \frac{K_{l,abs}\rho^2_w gAD(s+0.01)\left[e^{-A(s-c)}+e^{A(s-c)}\right]}{\mu_w m_w}\left(\frac{ds}{dz}\right) = 0 \quad (43)$$

Using the same approximation $D^{eff}_{N_2-w} \cong D^{eff}_{O_2-w}$, and inserting Eq. (31), Eq. (24) gives the form

$$\frac{P}{RT}\frac{dx_{O_2}}{dz} = -(1-x^s_w-x_{O_2})N_{O_2}\left[\frac{1}{D^{eff}_{N_2-O_2}} + \frac{x^s_w}{(1-x^s_w)D^{eff}_{O_2-w}}\right] \quad (44)$$

Inserting Eqs. (25) and (43) into Eq. (44) yields

$$\frac{dx_{O_2}}{(1-x^s_w-x_{O_2})} = -\eta\frac{(s+0.01)\left[e^{-A(s-C)}+e^{A(s-C)}\right]ds}{(1-s)^{1.5}} \quad (45)$$

where

$$\eta = \frac{K_{l,abs}RTADg\rho^2_w}{Pm_w\mu_w\varepsilon_0^{1.5}\left[2+4n_d+x^s_w/(1-x^s_w)-4\tau_wF/I\right]}\left[\frac{1}{D_{N_2-O_2}} + \frac{x^s_w}{(1-x^s_w)D_{O_2-w}}\right] \quad (46)$$

After integrating Eq. (45) over the two-phase region, one eventually arrives at

$$x^c_{O_2} = x^f_{O_2} - x^f_{N_2}\left[\exp(\eta\Lambda) - 1\right] \quad (47)$$

in which

$$\Lambda = -\int_{s^c}^{0}\frac{(s+0.01)\left[e^{-A(s-C)}+e^{A(s-C)}\right]}{(1-s)^{1.5}}ds \quad (48)$$

where s^c represents the water saturation at the diffusion-layer/catalyst-layer interface.

3.3. Performance equations

When an unsaturated air stream is employed as a cathode feed for a PEMFC, the amount of water transported from the exterior membrane boundary and generated by the oxygen reduction is usually not enough to fully hydrate the membrane and the ionomer phase in the catalyst layer at low current densities. The same situation might be encountered for a saturated air feed if a positive pressure difference is imposed between the two sides of the membrane. Under such a condition, liquid water is not present in the gas diffusion layer, and consequently the equations for case I should be employed for the calculations. As the current density is increased to a value beyond which the ionomer phase in the catalyst layer can be completely hydrated, liquid water starts to appear in the diffusion layer. For such an instance, the equations for case II are used in the computations.

After the water content profile within the membrane is calculated, the protonic conductance of the membrane is readily computed using Eq. (15). For the case that liquid water emerges in the diffusion layer, the membrane is fully hydrated; thus, one has

$$\sigma_m = (0.005139\lambda_s - 0.00326)\exp\left[1268\left(\frac{1}{303}-\frac{1}{T}\right)\right] \quad (49)$$

If liquid water is absent in the diffusion layer, the value of σ_m is estimated as an averaged value using

$$\sigma_m = \frac{1}{d_m}\int_0^{d_m}(0.005139\lambda - 0.00326)\exp\left[1268\left(\frac{1}{303}-\frac{1}{T}\right)\right]dz \quad (50)$$

Once the values of $x^c_{O_2}$, x^c_w, and σ_m become available, the cathode potential can be determined using the performance equations [36]:

$$V_c = V_o - \frac{I}{2\beta_1} - \frac{I}{\beta_2} - \frac{I}{\beta_m} - \frac{1}{f_c} \times \ln\left\{\frac{I+\beta_1/f_c[\exp(-If_c/\beta_1)-1]}{\varphi[I_o x^c_{O_2} - \beta_1/f_c + \exp(-If_c/2\beta_1)(\beta_1/f_c - I_o x^c_{O_2} + I/2)]}\right\} \times \text{for } I \le 2I_o x^c_{O_2} \quad (51)$$

$$V_c = V_o - \frac{I}{\beta_1} + \frac{x^c_{O_2}I_o}{\beta_1} - \frac{I}{\beta_2} - \frac{I}{\beta_m} - \frac{1}{f_c}$$

$$\times \ln\left\{\frac{I^2[2x^c_{O_2}I_o f_c - \beta_1 + \beta_1\exp(-2x^c_{O_2}I_o f_c/\beta_1)]}{4\varphi(x^c_{O_2})^2 I_o^2[x^c_{O_2}I_o f_c - \beta_1 + \beta_1\exp(-x^c_{O_2}I_o f_c/\beta_1)]}\right\}$$

$$\text{for } I \geq 2I_o x^c_{O_2} \quad (52)$$

in which

$$\beta_m = \frac{\sigma_m}{d_m} \quad (53)$$

The cathode potential expressions from Eqs. (51) and (52) can be viewed as the open-circuit value minus the individual potential losses stemming from the limitations of reactant transport, proton migration, electron conduction, and the electrochemical reaction. They were derived by assuming that the oxygen and ionomer potential profiles within the catalyst layer are parabolic polynomials (Eq. (51)) or piecewise parabolic polynomials (Eq. (52)). The switch between these two equations should be made as the oxygen depletion, computed using the prescribed profiles, occurs at the catalyst-layer/membrane interface. The procedures of their derivation and the expressions for the individual potential losses will not be presented here; readers interested in the details of the equation formulation are advised to consult the listed literature [36].

4. Results and discussion

The performance equations developed in the preceding sections were used to construct the discharges curves of PEMFC cathodes so as to investigate the effects of the model parameters on the cathode performance. Since the emphasis of the present work is on exploring the influence of water saturation within the diffusion layer on the cathode performance, only the analyses of certain model parameters whose changes may give rise to particular characteristics of liquid water transport within the diffusion layer will be included here. The parameter values listed in Table 1 are used in the calculations unless otherwise specified. It should be noted that the formulas and the parameter values for the capillary pressure of the gas diffuser were taken directly from the work of Natarajan and Nguyen [39] without any modifications. Different forms of capillary pressure based on other considerations have been also reported in the literature [40,41]. As shown in the procedures of the model formulation, the present approach is quite general and is not restricted to any particular forms of capillary pressure of the gas diffusion layer. Consequently, other expressions of capillary pressure can also be incorporated into the present performance equations without appreciable difficulties.

Fig. 2 demonstrates the discharge curves for cathode feeds with different relative humidities. Higher vapor content indeed favors an earlier saturation in the membrane and catalyst layer so that better proton conductivity is expected; as a result, high vapor saturation outperforms in the low current density region. For a better illustration of the hydration effect, the emergence of liquid water in the gas diffusion layer is marked in the figure. This point indicates the initial occurrence of a fully hydrated membrane and catalyst layer, before which the polymer membrane and the adjacent catalyst layer are only partially hydrated. The associated current density is determined by letting $d_w = 0$ in Eq. (38), and the oxygen mole fraction between one-phase and two-phase, $x^f_{O_2}$, can be calculated directly from Eq. (39). This oxygen concentration is equivalent to the interfacial concentration of CL/GDL $x^c_{O_2}$. The corresponding cathode voltage V_c is then determined either from Eq. (51) or (52) based on the criterion imposed on the calculated current density. Note that for RH = 1, full hydration commences from the open circuit potential for a steady-state operation. Before membrane saturation, ohmic resistance varies and decreases with discharged current until full hydration is arrived. As the membrane is saturated, liquid water flooding begins at the interface of the catalyst layer/gas diffusion layer. Liquid water in the gas diffusion layer obstructs the gaseous mass transfer of oxygen from the channel. Drier cathode feed results in a higher limiting current density due to a favorable gas diffusion of oxygen through the gas diffusion layer.

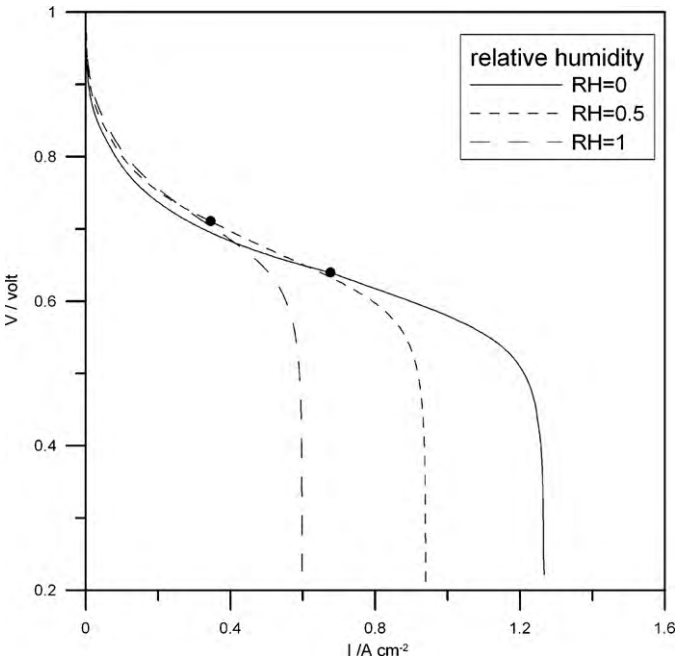

Fig. 2. Polarization curves at various cathode feed relative humidities. d_m = 50 μm, anode relative humidity = 1, cathode gas diffusion layer porosity = 0.5, diffusion layer liquid water permeability = 3×10^{-10} cm^2, $P^c = P^a$ = 5 atm, temperature 353 K. Solid symbols coordinates (0.3452, 0.7109), (0.6760, 0.6397) are conditions of emerging flooding in cathode gas diffusion layer for cathode feed relative humidities RH = 0.5 and 0, respectively.

The water saturation profiles corresponding to various current densities at the specified inlet RH = 0.5 are depicted in Fig. 3.

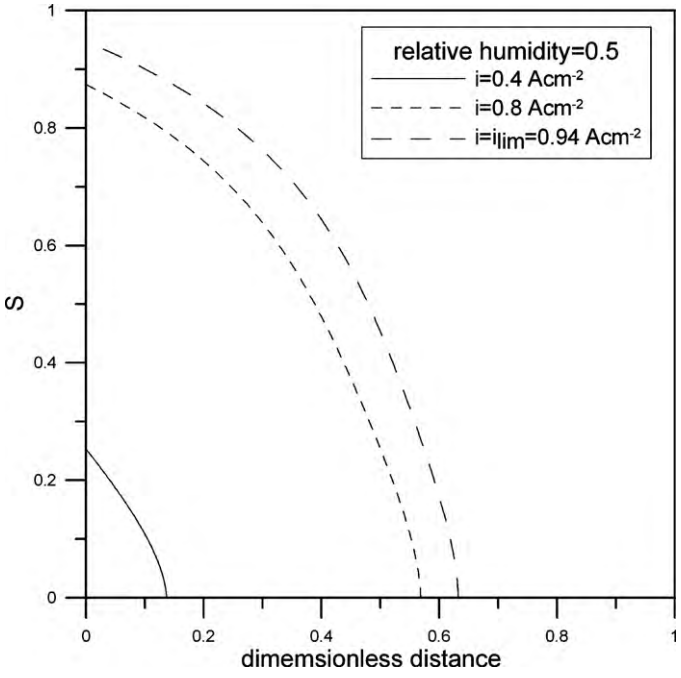

Fig. 3. Water saturation profiles in the gas diffusion layer at different discharge current densities for a specified cathode feed RH = 0.5. Other conditions are the same as that in Fig. 2.

Table 1
Values of model parameters.

Membrane thickness, d_m (cm)	0.005
Catalyst layer thickness, d_c (cm)	0.0005
Gas diffusion layer thickness, d_d (cm)	0.03
Effective electric conductivity in diffusion-layer and catalyst-layer, σ_d^{eff} (S cm^{-1})	1 [36]
Effective ionomer conductivity in catalyst layer in fully hydration, σ_m^{eff} (S cm^{-1})	3.1157×10^{-2}
Effective diffusivity of dissolved oxygen in the catalyst layer, $D_{O_2}^{eff}$ (cm^2 s^{-1})	1×10^{-5} [36]
Gas-pair diffusivity, $D_{O_2-N_2}$ (cm^2 s^{-1})	5.58×10^{-2}
Gas-pair diffusivity, D_{N_2-w} (cm^2 s^{-1})	7.74×10^{-2}
Gas-pair diffusivity, D_{O_2-w} (cm^2 s^{-1})	7.40×10^{-2}
Swelling expansion coefficient of membrane, e	0.0126
Porosity of gas diffusion layer at zero water saturation, ε_0	0.5
Volume fraction of the ionomer phase in the catalyst layer, ε_m	0.5
Product of platinum surface area and reference exchange current density, $a_0 i_{0,ref}$ (A cm^{-3})	1×10^{-2} [36]
Gas pressure, P (atm)	5 [36]
Saturated vapor mole fraction at 353 K, x_w^s (atm)	0.0934
Bulk oxygen to nitrogen molar ratio, $x_{O_2}^b / x_{N_2}^b$	21/79
Temperature, T (K)	353 [36]
Henry's constant, H_{O_2} (atm cm^3 mol^{-1})	2.04×10^5 [4]
Open circuit potential, V_0 (V)	1.2 [4]
Cathodic transfer coefficient, α_c	1.0 [36]
Hydraulic permeability of membrane, $k_{p,m}$ (cm^2)	1.58x10^{-14} [4]
Molar volume of dry membrane, v_m (cm^3 mol^{-1})	550
Molar volume of liquid water, v_w (cm^3 mol^{-1})	18
Water viscosity, μ_w (g cm^{-1} s^{-1})	3.565×10^{-3}
Density of liquid water, ρ_w (g cm^{-3})	0.972
Liquid water permeability in diffusion layer at fully hydration, $K_{l,abs}$ (cm^2)	3×10^{-10} [36]
Constants in capillary heat expression A, C, and D (cm)	3.7, 0.494 and 0.0173 [39]
Fully hydrated water content in membrane (mole of water per mole of sulfonic groups), λ_s	14.043 [7]

As shown, the water saturated domain in the gas diffusion layer expands along with the increased current density until the limiting condition is arrived. Since the assumption of instantaneous phase equilibrium is imposed in the model formulation, it is also desirable to discuss the characteristics of the inter-phase mass transfer of water molecules within the two-phase domain. Remember that for a fixed current density, N_{O_2} remains constant over the entire diffusion layer, as exhibited by Eq. (31). When the original Stefan–Maxwell equations are applied, under the presence of liquid water, the values of N_{O_2} and N_w are related by a function of x_w^s, x_{O_2}, and gas-pair diffusivities as revealed by Eq. (41). This indicates that small amounts of liquid water evaporate in the two-phase region since the value of x_{O_2} decreases monotonically towards the catalyst-layer/diffusion-layer interface. Nevertheless, the situation changes as the approximation $D_{N_2-w}^{eff} \cong D_{O_2-w}^{eff}$ is employed. Under such a condition, N_w remains unchanged in the two-phase region, as implied by Eq. (42). Consequently, evaporation of liquid water only occurs at the water saturation front. After liquid water vaporizes, a major portion of it continues to travel along the same direction to the gas channel, while the rest is dragged by the flow of oxygen to the catalyst-layer/diffusion-layer interface. It should be stated that in the work of Natarajan and Nguyen [39], a small number (0.01) was added to the water saturation in Eq. (28) so as to alleviate the infinitely large slopes at the water saturation front and to circumvent the numerical difficulties encountered in their computations. However, such an addition is not necessary in the present study since calculations with Eqs. (47) and (48) are still feasible without the presence of this small number.

The individual potential losses caused by the limitations of oxygen electrochemical reduction, oxygen mass transport, proton migration, electron conduction, and membrane ohmic drop for cathode feeds of relative humidities 0 and 1 are presented in Fig. 4. In general, the activation overpotential associated with oxygen reduction increases sharply as the current density is driven from the open circuit voltage. The rate of increase is alleviated as the current density is further raised. As a comparison, a higher activation overpotential is predicted when dry air is fed instead of air with saturated vapor. The membrane and the catalyst layer are more easily hydrated if a more humidified cathode feed is employed, and the activation overpotential is reduced due to a greater catalytic surface area being available for the electrochemical reaction. High inlet humidity also reduces the ohmic loss in the membrane and protonic ohmic loss in the catalyst layer due to greater hydration

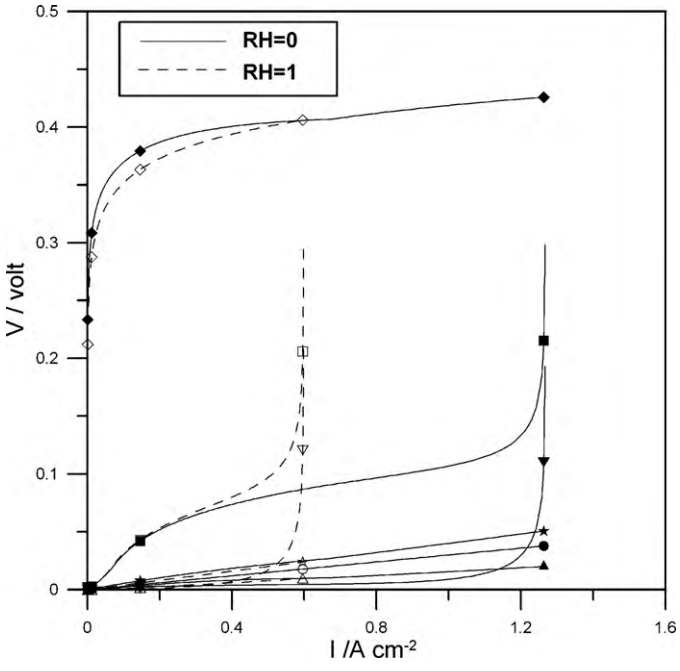

Fig. 4. Polarization curves of individual contributive terms calculated using performance equations at cathode feed relative humidities 0 and 1. (♦ ◊) Activation overpotential for oxygen reduction reaction, (▼ ▽) diffusion overpotential of catalyst layer, (▲ △) diffusion overpotential of gas diffusion layer, (● ○) ohmic potential loss of ionomer phase in catalyst layer, (■□) ohmic potential loss of gas diffusion layer, and (★ ☆) ohmic potential loss in the membrane. Open symbol for RH = 1, filled symbol for RH = 0. d_m = 50 μm, anode relative humidity = 1, cathode gas diffusion layer porosity = 0.5, diffusion layer liquid water permeability = 3×10^{-10} cm^2, $P^c = P^a$ = 5 atm, temperature 353 K.

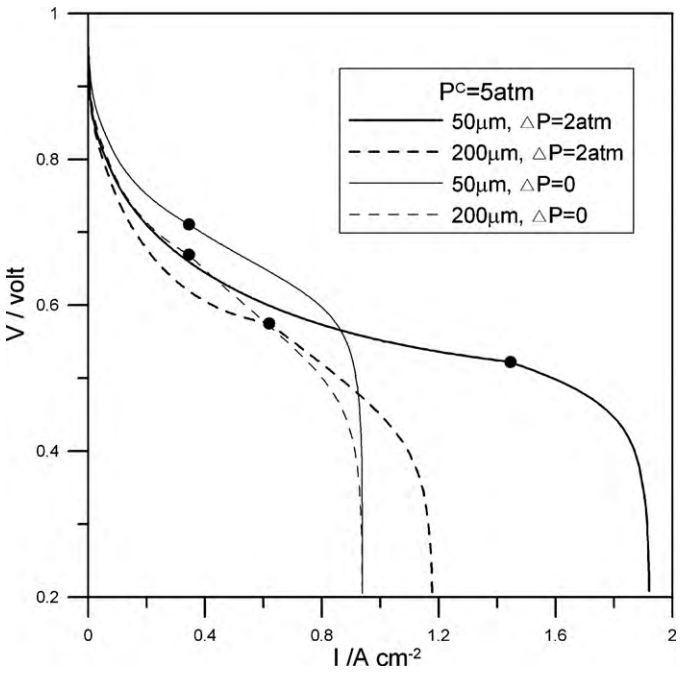

Fig. 5. Effect of membrane thickness and pressure difference between cathode and anode. Cathode pressure P^c = 5 atm. Anode relative humidity = 1, cathode feed relative humidity = 0.5, cathode gas diffusion layer porosity = 0.5, temperature 353 K. Solid symbols indicate the current densities of initial flooding in gas diffusion layer. (1.445, 0.5223), (0.6201, 0.5754) are for ΔP = 2 atm, membrane thickness 50 and 200 μm, respectively. (0.3452, 0.7109), (0.3452, 0.6694) are for ΔP = 0 atm, membrane thickness 50 and 200 μm, respectively.

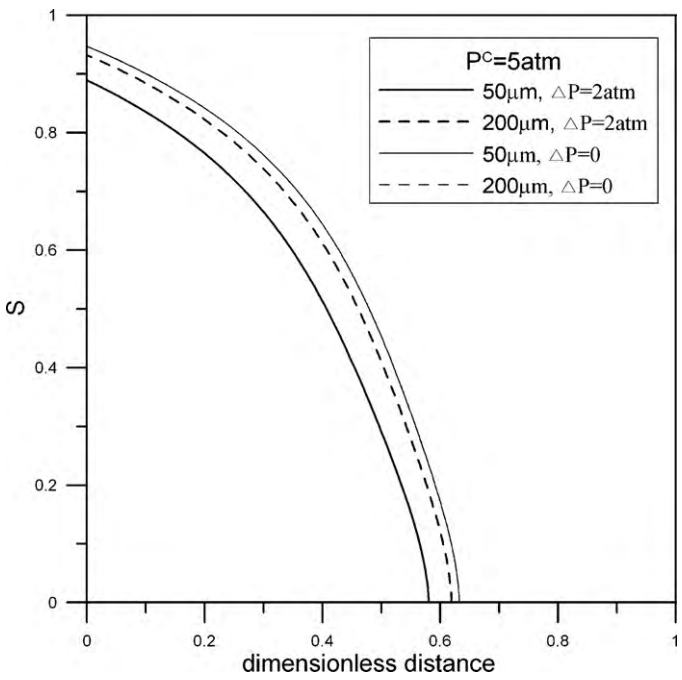

Fig. 6. Water saturation profiles at limiting current densities at various membrane thickness and pressure difference between cathode and anode. Cathode pressure P^c = 5 atm. Key is the same as that in Fig. 5.

in the ionomer phase, as indicated in Fig. 4. The major part of the overall ohmic loss of the cathode is caused by the proton migration in the ionomer phase of the catalyst layer and electron conduction in the gas diffusion layer. The potential loss in the gas diffusion layer is linearly proportional to the discharged current density. Oxygen is depleted in the cathode catalyst layer at high polarization, and the associated diffusion overpotential increases dramatically as the limiting current density is approached.

The effect of membrane thickness and the pressure difference between the cathode and anode, ΔP, is demonstrated in Fig. 5. An overall better performance is achieved when using a thinner membrane as a result of less ohmic resistance, better water diffusion rate in the membrane, and lower water saturation in the gas diffusion layer. The pressure effect differs at the low and high discharged regions. Higher values of ΔP prohibit the hydration of the membrane in the early stage, but prevent water flooding in the gas diffusion layer at high overpotential. Fig. 5 also shows that the back pressure is more influential if a thinner membrane is used because a greater pressure gradient is imposed. For instance, for a specified ΔP = 2 atm, a 50-μm membrane becomes fully hydrated at as high as 1.445 A cm^{-2}, in contrast to that of 0.6201 A cm^{-2} if a 200-μm membrane is used. The corresponding water saturation profiles at the limiting current condition are plotted in Fig. 6. A higher back pressure gradient prohibits the convective water flow and induces less water flooding in the cathode gas diffusion layer.

Fig. 7 demonstrates the effect of void fraction in the gas diffusion layer on the polarization curve at RH = 0.5. It shows that the membrane and the catalyst layer are saturated at a higher overpotential if a gas diffusion layer of greater porosity is used. There is also a slight performance enhancement in the low current density region for the diffusion layer with a low porosity due to better hydration of the membrane and the catalyst layer. As liquid water floods extensively within the diffusion layer, an MEA fabricated with larger gas pores allows for easier evaporation of liquid water and facilitates better water vapor diffusion; as a consequence, better cell performance results.

Fig. 8 evaluates the effect of liquid water permeability in the gas diffusion layer, $K_{l,abs}$, on the cell performance. Large values of $K_{l,abs}$ induce a facile convective mass transport of water, as suggested in the third term on the left hand side of Eq. (43); in consequence, lower water saturation is expected in the porous medium. Oxygen

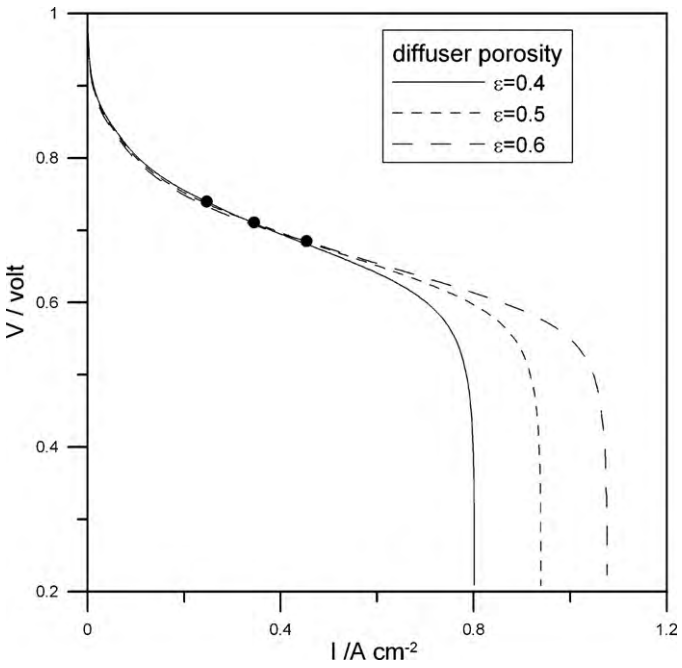

Fig. 7. Effect of gas diffusion layer void fraction on the cell performance. d_m = 50 μm, anode relative humidity = 1, diffusion layer liquid water permeability = 3×10^{-10} cm^2, $P^c = P^a$ = 5 atm, temperature 353 K. Coordinates (0.2470, 0.7398), (0.3452, 0.7109), and (0.4538, 0.6849) are the conditions of emergent flooding in gas diffusion layer for porosities 0.4, 0.5, and 0.6.

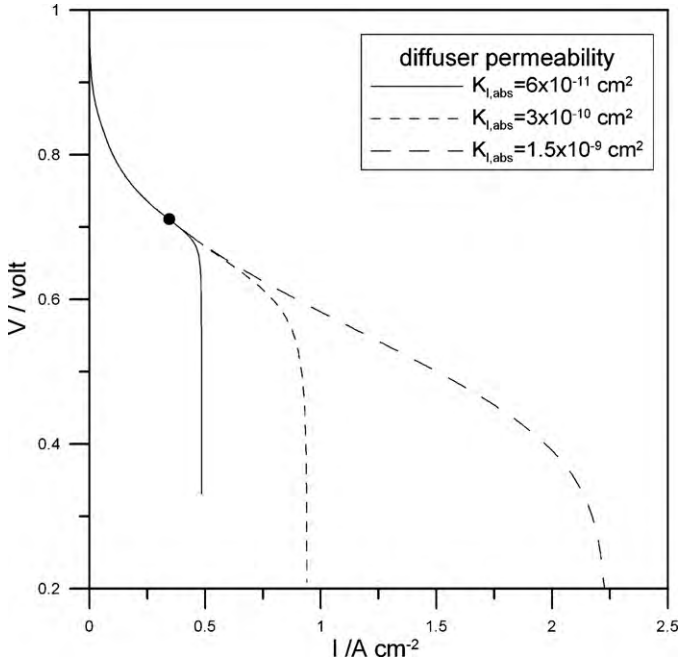

Fig. 8. Effect of diffusion layer liquid water permeability on the cell performance. d_m = 50 μm, anode relative humidity = 1, cathode gas diffusion layer porosity = 0.5, $P^c = P^a$ = 5 atm, temperature 353 K. (0.3452, 0.7109) is condition of emergence of flooding in gas diffusion layer.

transfer is more favorable when less gas void is blocked by the liquid water in the diffusion layer, as is most prominent in the high current density region. Note that before the emergence of liquid water at the membrane/catalyst-layer interface, cell performance is unaffected by the parameter $K_{l,abs}$.

5. Conclusions

Mechanistic performance equations of unsaturated cathode feed are derived for the cathode part of the MEA of a general PEMFC. Individual potential losses within the MEA can be assessed explicitly from first principles without the physical ambiguity that is encountered in empirical data fitting models. In the model, water transport in the membrane is described with electro-osmotic drag, diffusion, and pressure induced convection mechanisms in either partially or fully hydrated situations. Detailed oxygen and vapor concentrations in the diffusion layer, water contents in the ionomer phases within the membrane and catalyst layers, and the liquid water saturation profile in the diffusion layer are all well integrated in the analytical formulation. The interaction of Stefan–Maxwell type ternary gaseous diffusions and liquid water transport are correlated by the capillary equilibrium correlation within the porous medium. The model simulates PEMFC cathode performance from dry to fully humidified cathode feeds. Oxygen concentration and liquid water saturation distributions in the gas diffusion layer are explicitly determined for the specified current density and humidification. Computation of the performance equation is efficient, and is applicable to an extensive operating range, which allows for a better MEA design with desired physical/chemical properties.

Acknowledgements

The authors are grateful for research grants received from the Ministry of Education and National Science Council of the Republic of China (NSC 97-2221-E-155-028). The continuing financial support from NSC, without which the studies on fuel cells could never be possible, is indispensable for our research. The second author is indebted to Lili Cheng for her encouragement and assistance.

References

[1] J. Larminie, A. Dicks, Fuel Cell Systems Explained, Wiley, 2003.
[2] F. Barbir, PEM Fuel Cells: Theory and Practice, Elsevier, 2005.
[3] W. Vielstich, A. Lamm, H.A. Gasteiger, Handbook of Fuel Cells: Fundamentals Technology and Applications, vols. 1–4, Wiley, 2003.
[4] D.M. Bernardi, M.W. Verbrugge, AIChE J. 37 (1991) 1151.
[5] D.M. Bernardi, M.W. Verbrugge, J. Electrochem. Soc. 137 (1990) 3344.
[6] D.M. Bernardi, M.W. Verbrugge, J. Electrochem. Soc. 139 (1992) 2477.
[7] T.E. Springer, T.A. Zawodzinski, S. Gottesfeld, J. Electrochem. Soc. 138 (1991) 2334.
[8] T.E. Springer, M.S. Wilson, S. Gottesfeld, J. Electrochem. Soc. 140 (1993) 3513.
[9] C. Marr, X. Li, J. Power Sources 77 (1999) 17.
[10] Q. Wang, M. Eikerling, D. Song, Z. Liu, T. Navessin, Z. Xie, S. Holdcroft, J. Electrochem. Soc. 151 (7) (2004) A950.
[11] K. Broka, P. Ekdunge, J. Appl. Electrochem. 27 (1997) 281.
[12] M.L. Perry, J. Newman, E.J. Cairns, J. Electrochem. Soc. 145 (1998) 5.
[13] F. Jaouen, G. Lindbergh, J. Electrochem. Soc. 150 (12) (2003) A1699.
[14] K.-M. Yin, J. Electrochem. Soc. 152 (3) (2005) A583.
[15] K.-M. Yin, J. Appl. Electrochem. 37 (2007) 971.
[16] K. Hongsirikarn, X. Mo, Z. Liu, J.G. Goodwin Jr, J. Power Sources 195 (2010) 5493.
[17] W.-M. Yan, F. Chen, H.-Y. Wu, C.-Y. Soong, H.-S. Chu, J. Power Sources 129 (2004) 127.
[18] L. Matamoros, D. Bruggemann, J. Power Sources 161 (2006) 203.
[19] R. Bradean, K. Promislow, B. Wetton, Numer. Heat Transfer A 42 (2002) 121.
[20] J.J. Hwang, J. Power Sources 161 (2007) 174.
[21] C.-H. Min, J. Power Sources 195 (2010) 1880.
[22] C.J. Bapat, S.T. Thynell, J. Power Sources 185 (2008) 428.
[23] C.J. Bapat, S.T. Thynell, J. Power Sources 179 (2008) 240.
[24] H. Meng, C.-Y. Wang, Fuel Cells 4 (2005) 455.
[25] X.-D. Wang, Y.-Y. Duan, W.-M. Yan, X.-F. Peng, J. Power Sources 175 (2008) 397.
[26] M.-S. Chiang, H.-S. Chu, C.-K. Chen, S.-R. Jian, J. Power Sources 166 (2007) 362.
[27] G.-S. Kim, P.C. Sui, A.A. Shah, N. Djilali, J. Power Sources 195 (2010) 3240.
[28] E.A. Ticianelli, C.R. Derouin, A. Redondo, S. Srinivasan, J. Electrochem. Soc. 135 (1988) 2209.
[29] J. Kim, S.M. Lee, S. Srinivasan, C.E. Chamberlin, J. Electrochem. Soc. 142 (1995) 2670.
[30] S. Hirano, J. Kim, S. Srinivasan, Electrochim. Acta 42 (1997) 1587.
[31] G. Squadrito, G. Maggio, E. Passalacqua, F. Lufrano, A. Patti, J. Appl. Electrochem. 29 (1999) 1449.
[32] D. Chu, R. Jiang, C. Walker, J. Appl. Electrochem. 30 (2000) 365.
[33] Z.T. Xia, S.H. Chan, Int. J. Hydrogen Energy 32 (2007) 878.
[34] H.-K. Hsuen, J. Power Sources 123 (2003) 26.
[35] H.-K. Hsuen, J. Power Sources 126 (2004) 46.
[36] H.-K. Hsuen, J. Power Sources 137 (2004) 183.
[37] A.J. Bard, L.R. Faulkner, Electrochemical Methods, Wiley, New York, 1980.
[38] I.-M. Hsing, F. Peter, Chem. Eng. Sci. 55 (2000) 4209.
[39] D. Natarajan, T.V. Nguyen, J. Electrochem. Soc. 148 (2001) A1324.
[40] U. Pasaogullari, C.Y. Wang, J. Electrochem. Soc. 151 (3) (2004) A399.
[41] U. Pasaogullari, C.Y. Wang, Electrochim. Acta 49 (2004) 4359.